Supergrowth of Nitrogen-Doped Single-Walled Carbon Nanotube Arrays: Active Species, Dopant Characterization, and Doped/Undoped Heterojunctions

Cary L. Pint,[†,§,*] Zhengzong Sun,[†] Sharief Moghazy,[†] Ya-Qiong Xu,[‡] James M. Tour,[†] and Robert H. Hauge[†,*]

[†]Department of Chemistry and Richard E. Smalley Institute of Nanoscale Science and Technology, Rice University, Houston, Texas, United States, and [‡]Department of Physics and Department of Electrical Engineering, Vanderbilt University, Nashville, Tennessee, United States. [§]Present address: Intel Corporation, Santa Clara, California, United States.

ABSTRACT We demonstrate the water-assisted supergrowth of vertically aligned single-walled carbon—nitrogen nanotubes (SWNNTs) using a simple liquid/gas-phase precursor system. *In situ* characterization of gas-phase nitrogen-containing precursors and their correlation to growth identifies HCN as the most active precursor for SWNNT growth, analogous to C_2H_2 for single-walled carbon nanotubes (SWNTs). Utilizing Raman spectroscopy, combined with XPS and *in situ* mass spectrometry during growth, we demonstrate the ability to probe N atoms at low concentrations (10^{-5} at. % N) in the SWNNT. Additionally, we demonstrate sensitivity of SWNNT optical transitions to N-doping through absorbance measurements, which appear to be a sensitive fingerprint for SWNNT doping. Finally, we demonstrate the fabrication of SWNT/SWNNT heterojunctions in the self-assembled carpet morphology that can be printed to arbitrary host substrates and facilitate potential emerging applications for this material. This work brings together new aspects regarding the growth, characterization, and materials processing that can yield advanced material architectures involving electronically tuned SWNNT array networks.

KEYWORDS: chemical vapor deposition · carbon nanotubes · carpets · nitrogen doping · HCN · heterojunction · Raman spectroscopy

Substitutional doping of charged impurities into conventional semiconductor materials has revolutionized the uses and applications of these materials in the past century. Growth of self-assembled nanomaterials, with nanostructured components individually substitutionally doped, can yield nanomaterial platforms that collectively operate with greater efficiency than conventional materials in a broad range of applications. Carbon nanotubes (CNT) are ideal for such applications, since n- or p-type doping has been demonstrated in both single-walled carbon nanotubes (SWNTs)[1−8] and multiwalled carbon nanotubes (MWNTs),[9−22] and synthesis of self-assembled CNT materials has been readily achieved. This general idea has fostered excitement about applications, such as for architectures that could be integrated into photovoltaics designs[9] and applications in electrocatalysis,[10] concepts currently at the forefront of CNT-based research.

Supergrowth[23,24] approaches have elevated the promise of SWNT utility for diverse applications. Supergrowth is a general process by which ultralong, densely packed (up to several millimeters) SWNTs are grown in the presence of oxygen-containing species (typically H_2O), where the precursor mixture aids to both clean amorphous carbon products[23,24] and enhance the catalyst lifetime.[25,26] An inherent feature of supergrowth is the fixation of the catalyst layer to the base of the growing array, allowing metal-free and removable self-assemblies of aligned SWNTs for applications,[27] a feature not achievable through many growth processes yielding poorer quality doped MWNT arrays with metal catalyst distributed through the network (and often introduced throughout the growth process). In addition, the doping of N atoms into the lattice relies upon precursor chemistry that has not been well studied or understood. Although recent studies have emphasized exciting concepts regarding the species that are present in CNT growth particularly from C_2H_4/H_2[28,29] and also demonstrated the enhancement of growth occurring from species that form as byproducts of C_2H_4,[30,31] fundamental knowledge of efficient routes to dope CNTs or SWNTs with known precursor chemistries has not yet been established.

* Address correspondence to cary.l.pint@intel.com, hauge@rice.edu.

Received for review April 4, 2011 and accepted August 6, 2011.

Published online August 07, 2011
10.1021/nn201252z

Furthermore, vertical array growth of doped high-quality SWNTs has not yet been demonstrated, as integrating N atoms into the wall of a SWNT represents a substantially more complex issue compared to that of a MWNT due to the necessity of a controlled precursor chemistry. However, substitutional doping in SWNTs grown in entangled morphologies has been achieved with a variety of dopants, including nitrogen, boron, silicon, and phosphorus.[1−3,7,8] The challenge to studying these materials has been analysis of the dopant presence and concentration.[1,4,5,32] The use of X-ray photoelectron (XPS) and electron energy loss (EELS) spectroscopies has proven effective at high dopant concentrations (>1 at. %),[5,13,15] which is already excessive in most cases. Recent work[33] has demonstrated the sensitivity of the G′ mode in Raman to the dopant presence, but this technique remains qualitative relative to the dopant concentration.[2] Therefore, a number of issues emerge with respect to advancing this material into applications. As a means to understand the growth process and manipulate it to yield controlled doping, one must identify "active species" in substitutionally doped SWNT growth to engineer the most efficient and controllable growth process. As a next step, one must have multiple tools designed to characterize the doped SWNTs and quantitatively assess both the dopant concentration over a range of dopant densities and nanotube physical properties relevant to applications. Finally, one must envision and employ techniques to incorporate doped SWNT materials into the framework of an application. Therefore, the purpose of this work is to provide important progress on each of these concepts while demonstrating a new embodiment of supergrowth that acts to produce high-quality and ultralong nitrogen-doped SWNTs (SWNNTs). In brief, this work (i) identifies HCN as an active precursor for N-doped SWNT supergrowth, (ii) demonstrates sensitivity of optical characterization to N-doping and emphasizes the use of excitonic signatures to quantitatively characterize N-doping (down to 10^{-5} at. % N-content), and (iii) demonstrates the robust nature of supergrowth to easily fabricate SWNT/SWNNT heterojunctions having built-in rectifying interfaces and with array morphologies that can be printed to host substrates for direct application development.

RESULTS AND DISCUSSION

SWNNT Supergrowth. A fundamental principle of achieving this technique is the controllable introduction of the N-containing precursor into the gas-phase chemical vapor deposition system during supergrowth. This is achieved using a similar approach[34] to a recent study where hydrazine was introduced to the CVD system for low-temperature gas-phase catalyst reduction and is illustrated in Figure 1a. This technique utilizes N-containing precursors with high vapor pressures of N-containing small molecules that include pyridine (C_5H_5N) and acetonitrile (CH_3CN), whose vapors can be metered into the reaction gas flow to achieve controllable and highly reproducible levels of N-doping by fixing the partial pressure of the precursor. To achieve moderate or low N concentrations, the N-containing precursor is mixed with acetylene, whereas for high N concentrations, the N-containing precursor is the only carbon species present. Shown in Figure 1b is a scanning electron microscope (SEM) image of a short SWNNT carpet (~20 μm) and a longer (~1.5 mm) SWNNT carpet obtained in this growth process with mixtures of CH_3CN and C_2H_2. Details on these techniques are available in the Methods section, though we note that both contain ultralong and N-doped SWNTs. A maximum height of ~1.5 mm is achieved in 60 min using this technique, even though the variation of height near chip edges indicates that changes in flow direction[23] (and carbon precursor) could substantially increase SWNT length and yield. Nonetheless, to study the SWNNT array growth process, we mainly focus our efforts on the shorter carpet species (<100 μm), which grow with good homogeneity in height and SWNT properties (relative to position in the carpet) and are therefore easier to controllably obtain and reproducibly characterize.

Transmission electron microscopy (TEM, Figure 2) was performed on a variety of as-grown SWNNT samples, each having different N-concentrations and grown with different precursors. Overall, TEM images emphasize that all observed tubes are single-walled with a standard supergrowth diameter distribution (1−5 nm, average ~3 nm) and remain relatively clean of amorphous carbon species. The latter point is also evident from Raman spectra (Supporting Information), which emphasizes a G/D ratio of ~10, emphasizing good wall quality that is consistently observed until very high doping levels. This is also typical of the pure SWNT product obtained in the supergrowth process based on previous TEM, AFM, and IR absorbance measurements.[24,27] The at. % of N-content is assigned on the basis of data and analysis presented later in this work. Extensive TEM imaging indicates the presence of only SWNNTs, with no DWNNTs or MWNNTs observed, and no presence of metal catalyst. In addition, no observable shift in SWNNT diameter (or wall quality) with N concentration is evident from this imaging, which is consistent with the idea that the catalyst nanoparticle diameter should not change upon N presence and that the nanoparticle size dictates SWNNT diameter, similar to SWNT growth. This imaging therefore confirms the presence of SWNNTs, consistent with SWNT achieved in supergrowth, and provides the basis for investigations into the growth, characterization, and applications of these materials described herein.

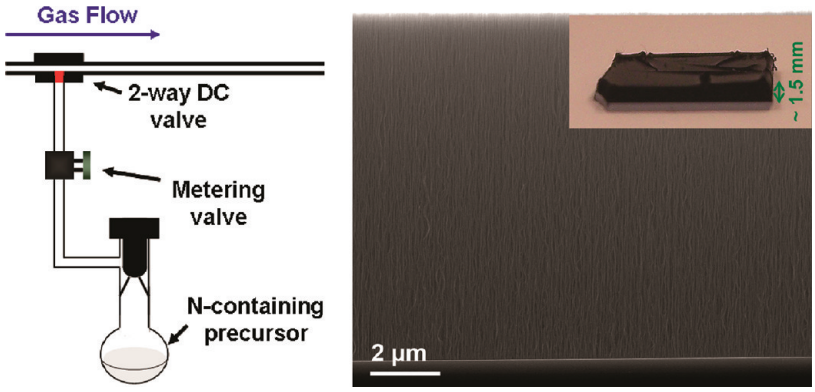

Figure 1. (a) Scheme depicting the experimental approach for supergrowth with gas-phase N-containing precursors and (b) SEM image of a vertically aligned SWNNT array (with photograph of a 1.5 mm long SWNNT array inset).

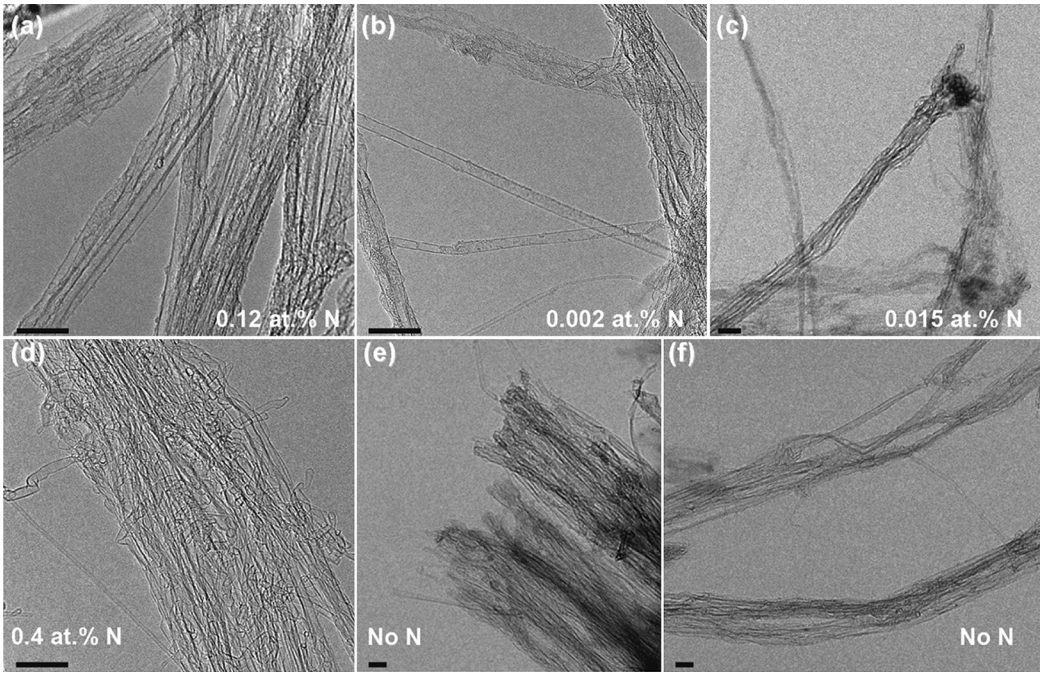

Figure 2. HR-TEM characterization of SWNNTs and SWNTs grown using this technique, including SWNNTs with (a) 0.12 at. % N using a C_5H_5N precursor, (b) 0.002 at. % N using a C_5H_5N/C_2H_2 precursor, (c) 0.015 at. % N using a CH_3CN/C_2H_2 precursor, (d) 0.4 at. % N using a CH_3CN precursor, and (e, f) pristine SWNT using C_2H_2. Note: scale bar = 20 nm.

HCN as the Active SWNNT Growth Precursor. One of the most important things to identify when considering the growth of SWNNTs is the active carbon species yielding the most efficient growth and, in this case, the most efficient N-doping. In recent studies with pure carbon precursors, it has been demonstrated that acetylene is significantly more efficient for SWNT array growth in chemical vapor deposition (CVD) compared to other known precursors.[35−39] Furthermore, recent studies have emphasized that CVD growth with ethylene produces triple-bonded carbon (acetylene) species in thermal decomposition that are most active in promoting high-yield CNT growth.[30] In this spirit, we utilized *in situ* mass spectrometry during growth and thermal annealing to investigate the decomposition of C_5H_5N and CH_3CN in order to determine whether these precursors are independently responsible for the N-doping or whether decay routes to prime active species exists that are products of precursor decomposition. To perform this, we utilized a mass spectrometer housed in an ultrahigh vacuum chamber (base pressure 1×10^{-9} Torr) connected to our growth system with a small bleed line connected to the SWNT growth furnace exhaust. More details on this experimental setup is discussed in the Supporting Information. Results from mass spectrometry (Figure 3) are shown in three unique cases: (i) a control experiment with no precursor and only H_2/H_2O and background species, (ii) a high partial pressure of N-containing precursor (T = 750 °C), and (iii) the same case as (ii), except with a hot tungsten filament. As will be shown

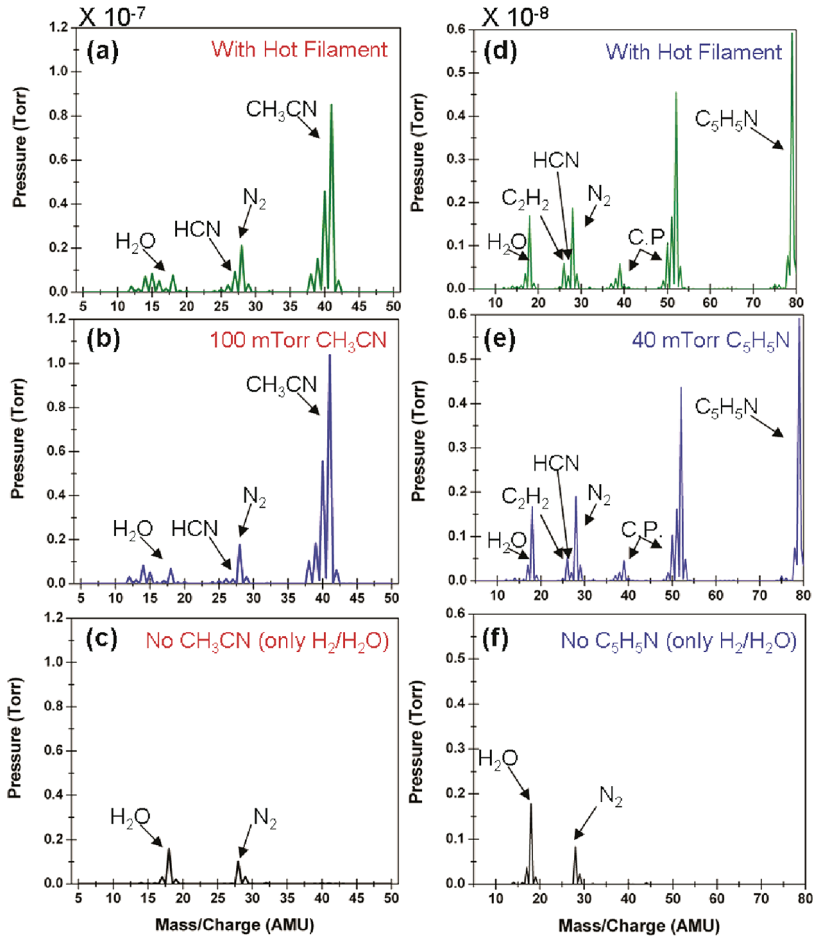

Figure 3. Mass spectrum analysis for (a–c) CH_3CN thermal decomposition and (d–f) C_5H_5N thermal decomposition. Arrows point to key peaks to consider, while C.P. refers to peaks arising from known molecular cracking patterns. Unlabeled peaks are primarily attributed to cracking patterns.

later in this work, the case in (iii) leads to the greatest N-doping, at least an order of magnitude more than without the filament use (for CH_3CN). However, detailed analysis of this data emphasizes an interesting feature, which is the presence of a *m*/*c* ratio of 27 that appears to be significantly enhanced when the hot filament is energized. The appearance of this peak only when the hot filament is energized, and independent of other peaks, suggests it is not a fragment from the electron ionization mass spectrum of a larger species (such as C_2H_4), but rather it is HCN. It should be noted that there is possible overlap of other species in some peaks, such as the *m*/*c* = 28 peak. Although we attribute most of this peak to N_2, a small portion of it could also be due to CO presence, which has an indistinguishable cracking pattern. Nonetheless, CO should not be reactive with the catalyst or the precursor species under the conditions described here, and so we have just labeled this peak independently as N_2, as it does not influence the relative analysis of the peak corresponding to HCN. For both CH_3CN and C_5H_5N gas-phase precursors, a significant portion of the thermal decomposition product is known to be HCN.[40,41] In fact, the toxicity of CH_3CN to humans can be related to secondary HCN production. However, HCN has a unique triple C–N bond analogous to other known efficient carbon precursors for CNT growth.[30] It is also perhaps of concern that one can observe a small C_2H_2 peak in the mass spectrum (primarily in C_5H_5N decomposition), but in both cases, this is invariant with hot filament exposure and completely accounted for by the cracking pattern of the N-containing precursor. Control experiments (described at length in the Supporting Information) to determine any effect of C_2H_2 production on growth suggest that if C_2H_2 is utilized at a level matching the partial pressure of the fragment in the electron ionization mass spectrum, only 50% of the growth is achieved as compared to an experiment using CH_3CN and no C_2H_2. This suggests that any secondary C_2H_2 production plays a negligible effect on the catalytic activity in comparison to the HCN species, since we know that the majority of the *m*/*c* = 26 peak is due to the cracking pattern of the N-containing precursor species. Furthermore, additional control studies were

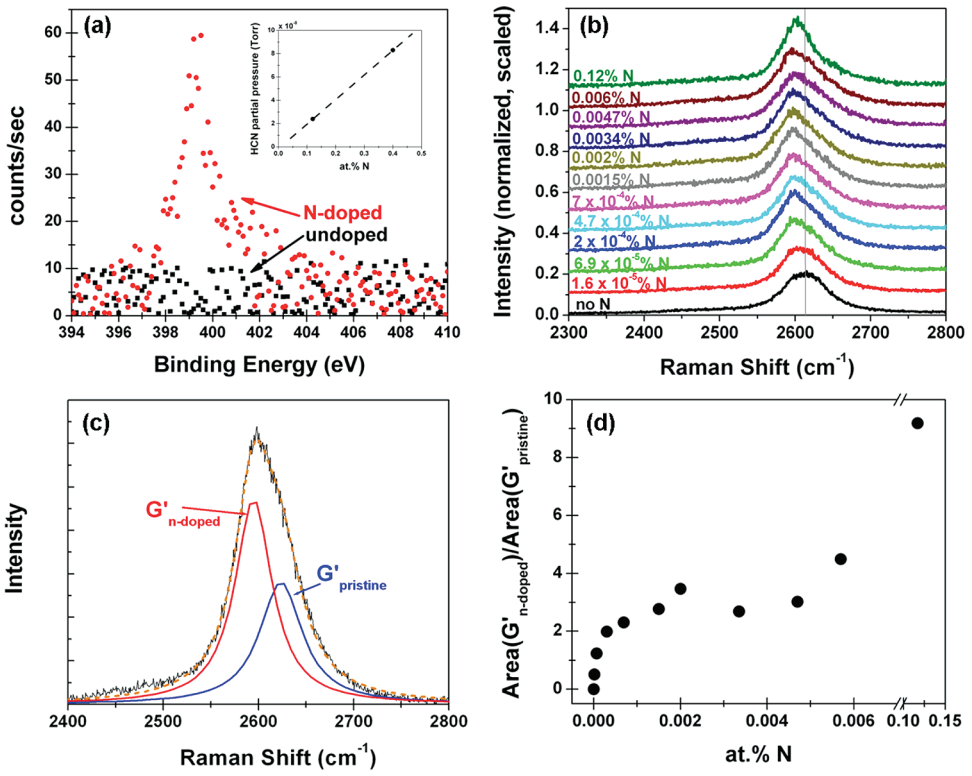

Figure 4. (a) XPS characterization of SWNNTs grown purely with CH_3CN (red) and C_2H_2 (black) to emphasize N presence and quantitatively determine N-content, with inset plot depicting the extrapolation for N-content assignment based on mass spectrometry measurements and XPS characterization. (b) Raman spectroscopy characterization of the G′ double resonance mode with increasing N-content with 633 nm excitations. N-content is assigned in at. % based on combined XPS and mass spectrometry data. (c) Fitting routine showing the double-Lorentzian peak fitting to quantitatively analyze N-content. (d) Ratio of the G′ contributions from n-doped SWNTs and that from pristine SWNTs.

conducted to correlate the production of HCN (which is described in Figure 3) to the growth process. The results are clear in that growth in both cases (at 1.4 Torr) without the hot filament is either not apparent by the eye or else results in a light browning on the surface. Energizing the hot filament yields the production of HCN species as demonstrated by the mass spectrometry (Figure 3b and e) and in both cases yields good catalytic activity and aligned N-doped SWNT arrays with CH_3CN precursors yielding the best efficiency due to the increased HCN production (Figure 3b). In these experiments, care was taken to keep the samples a reasonable distance from the filament to mitigate the formation of atomic hydrogen from the filament. Therefore, we can relate efficient SWNNT growth to the production of HCN active species in the CVD reactor based on these experiments and analysis. Considering past work with N-doped SWNTs or MWNTs, standard precursors such as benzylamine[15] or pyrizine[2] are also similarly expected to decompose at high temperatures to yield a small percentage of HCN. Recent studies suggest[15] that higher temperatures during growth lead to more efficient N-doping of few-walled CNTs. We speculate that this could be consistent with increased HCN production due to thermal decomposition of the active precursor, which is the source of HCN production in our growth system. This provides a universal function of a precursor for SWNNT growth with these precursors, which is to efficiently produce HCN. The unique role in triple-bonded carbon species for efficient CNT growth is interesting and could be related to C−N or C−C dimer formation that can migrate across a catalyst and efficiently fit into vacant sites in a growing SWNT or SWNNT. However, we only find SWNNTs having a maximum doping level of 0.4 at. %, compared to the 50 at. % expected if all N was retained from HCN. Therefore, we postulate that efficiently doping CNTs with N is related to (i) the efficient production of a universal HCN species active for SWNNT growth and (ii) the kinetics of the C and N species on the catalyst that dictate the ratio of N added to the carbon lattice. Thus, this yields a rational approach to substitutionally dope SWNTs with nitrogen from triple-bonded C−N species, and we therefore postulate on the basis of this work that efficient growth and doping can be achieved from carbon-containing molecules with a similar structure to C_2H_2 and HCN.

Characterization of SWNNTs. Possibly the most important aspect of growing SWNNTs is the ability to

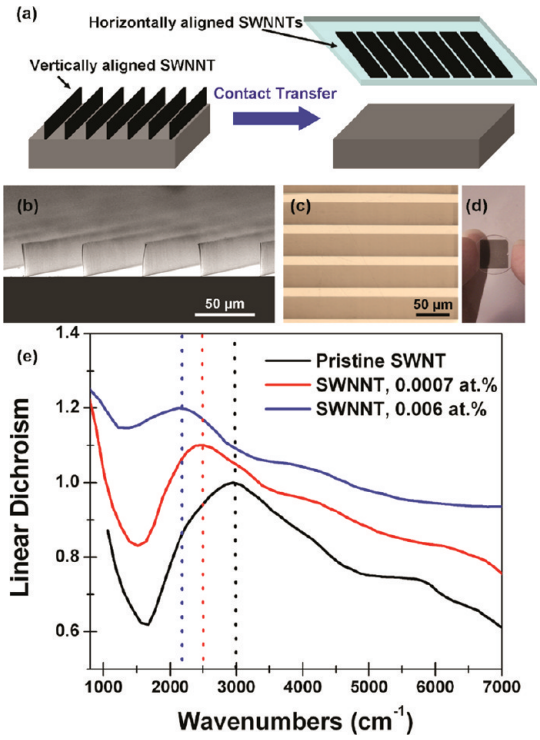

Figure 5. (a) Scheme depicting the contact transfer process utilized for preparing horizontally aligned (HA) SWNNT samples for polarized optical absorption experiments. (b) SEM image of upright SWNNT lines following growth. (c) Optical microscope image of transferred HA-SWNNTs. (d) Photograph of a ~1 cm × 1 cm pattern of HA-SWNNTs transferred to a circular KBr window. (e) Linear dichroism (scaled on *y*-axis) for pristine SWNT and two different SWNNT concentrations, showing the red-shift of the E_{11}^{sc} optical absorption.

accurately characterize the physical properties of the tubes (defect quality, diameter, *etc.*) as well as the N-content. Presently, quantitative assessment of N-content is achievable only at high dopant concentrations (>~0.2 at. % N) *via* XPS and EELS,[4,5,13,15] whereas the limit of N by which other qualitative techniques, such as Raman spectroscopy, are effective has not been established. Figure 4a shows XPS spectra from the highest doped SWNNT array in this study, which yields a concentration of ~0.4 at. % N based on a comparison of peak heights normalized to the respective X-ray cross section. We note that lower concentrations (≤0.1 at. % N) are below the noise level in the spectra. The N1s peak position is at ~399.5 eV, which is between the pyridine (398.5 eV) and sp^2 N (400.5 eV) binding energies,[15] suggesting a nearly equal presence of both types of N coordination in the SWNNT. Utilizing this information, we can simply relate the HCN concentration from mass spectrometry to the nitrogen content in the SWNNT by correlating the HCN peak to the XPS data and extrapolating this to lower N concentrations that cannot be measured using XPS (inset, Figure 4a). When C_2H_2 is cooperatively utilized as a precursor, we simply assume a dilution of N based on HCN and C_2H_2 levels measured in mass spectrometry. This approach is approximate, but allows us to assign relative N-content down to levels immeasurable by all techniques employed here.

Optical characterization of SWNNTs is performed in this study using two techniques: Raman spectroscopy characterization and infrared absorption (Figures 4b–d and 5). Of these, qualitative signatures of N-doping only recently have been demonstrated using Raman spectroscopy.[33] This is based on characterization of the double-resonance G′ mode, which is sensitive to electronic interaction with charged species occupying SWNT lattice sites. As shown in Figure 4b, these SWNNT arrays show a strikingly similar red-shift in the G′ mode (633 nm excitation) with increasing N-content, validating the concept of controlled SWNNT supergrowth. However, a distinguishing feature of our work is the ability to assign SWNT N-content to the onset of a significant $G'_{N\text{-doped}}$ component of this peak based on a correlation between XPS data and mass spectrometry results. We therefore find that the G′ mode is sensitive to N-doping levels down to 10^{-5} at. % N, nearly 4 orders of magnitude lower than XPS or EELS can effectively estimate N-content. Furthermore, plotting the peak area of the $G'_{N\text{-doped}}$ peak compared to the G'_{SWNT} peak area as a function of concentration (using both C_5H_5N and CH_3CN precursors), a somewhat scattered linear relationship is uncovered (Figure 4d) for all points that are not strongly influenced by fitting error (all points on the line). This emphasizes not only that the G′ mode can be an effective tool for quantitative N-content analysis but that our technique for assigning at. % N is reasonable. It should be noted that our analysis is based on the approximation that the relationship between the active precursor species and the N-content at high doping levels (>0.4 at. %) is valid at orders-of-magnitude lower doping levels. Future studies will need to be conducted to further quantify this relationship, which is dependent upon the chemical mechanism for N atom incorporation into the SWNT lattice. In this spirit, we envision the specific approach here to give us a crude estimate into N atom content at levels that were previously immeasurable, and we emphasize the use of this general technique with further refined relationships between the N-content and the active precursor concentration as a highly accurate way of analyzing dopant concentration in nanocarbon materials. Nonetheless, based on the results we present here, it is clear that Raman spectroscopic characterization can effectively be utilized as a sensitive fingerprint for doping at levels in the range of 10^{-5} at. % N, which covers the range of dopant concentrations useful for the development of applications from this material.

As an alternative to Raman spectroscopy, the characterization of SWNTs in the supergrowth diameter range can be carried out most effectively utilizing absorption studies.[27] Recent pioneering theoretical

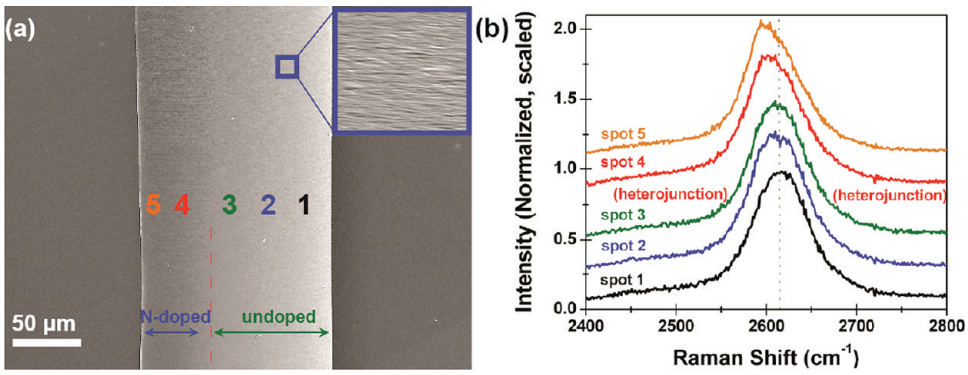

Figure 6. (a) SEM image of a single ~130 μm long HA-SWNNT/SWNT made by rapidly introducing CH_3CN into the C_2H_2 flow. The contrast difference on each side evidences the presence of self-assembled molecular heterojunctions, with the N-doped and pristine sides labeled. (b) Raman mapping of the heterojunction in (a), with spots corresponding to the labeled spots in part (a).

advances have predicted the sensitivity of band gaps and many-body excitonic effects to doping of SWNTs,[42] even though experiments have yet to characterize such materials carefully. This has motivated our efforts to establish sensitive fingerprints for N-doping using polarized infrared (IR) absorption studies on aligned SWNNT species. Recent studies have shown that IR absorption for pristine SWNTs is capable of rapidly yielding a diameter distribution by analysis of optical transition energies of semiconducting SWNTs.[27] Here, we perform a similar approach, by utilizing patterned arrays of SWNNTs, contact transfer of well-aligned SWNNT films to IR-transparent KBr windows, and characterizing the linear dichroism (Abs(∥) − Abs(⊥)) using polarized absorption. This process and spectra are shown in Figure 5a−e. As noted in Figure 5e, there is a red-shift of the peak corresponding to the E_{11} semiconductor (E_{11}^{SC}) optical transition. This red-shift is found to be consistently enhanced by increasing N-content in the SWNNT. The decrease in the linear dichroism (note that data are stacked in Figure 5e to emphasize the change in E_{11}^{SC} peak position) with N-content can be related to decreased anisotropy occurring from lower growth rates with higher N-content. This is likely an artifact of the transfer process, yielding less aligned material relative to the edge of the lines of SWNNTs, where the nanotubes are often misaligned due to the nature of the transfer process. Nonetheless, we observe that for an N-content of 0.006% and an average SWNT diameter of ~2.7 nm (which is generally invariant based on TEM characterization), a red-shift of ~100 meV is observed relative to pristine SWNT. It should be noted that modification of excitonic transitions based on N-doping should be a diameter-dependent phenomenon since more atoms are incorporated in the lattice per unit nanotube length for larger diameter SWNNTs. It is also interesting that theoretical predictions suggest that doping not only simply influences gap energies but also modifies many-body effects (such as the exciton binding energy).[42] In any case, the use of well-defined absorption features consistent with N-doping could prove to be an important tool, in concert with Raman spectroscopy, to quantify N-doping at low levels of N-content in SWNNTs.

SWNNT/SWNT Heterojunctions. An intrinsic feature of supergrowth is the synthesis of ultralong SWNT from a catalyst layer that remains pinned at the base of the substrate during growth. This feature, combined with the ability to grow SWNNTs and transfer self-assembled patterns of aligned SWNNTs to host surfaces, yields a unique "bottom-up" approach for growing nanostructures that can be engineered for applications. As we show in Figure 5, N-doping can be utilized as a tunable "knob" for modifying the dopant content, and hence electronic characteristics, of the SWNNT arrays. Therefore, we demonstrate the fabrication of a novel heterostructure format that involves N-doped and undoped sections along the length of ultralong SWNTs that are self-assembled into thin (~1 μm thick, ~130 μm long) lines transferred and laid over[27,43] on host surfaces (one example shown in Figure 6a). This structure is made by nucleating with a C_2H_2 feedstock, growing for 5 min, and then continuing the growth with a mixture of C_2H_2 and CH_3CN for 30 min. Such a routine should not disrupt the growth and should lead to ultralong continuous SWNTs that are partially doped with N and partially pristine. The unique feature of this structure is the abrupt interface between the SWNNT side and the SWNT side, which is visible in Figure 6a by contrast in the SEM, but also more apparent through Raman mapping of the G′ mode using 633 nm laser excitations in Raman spectroscopy (Figure 6b). Although the Raman mapping is not capable of characterizing the microscopic interface between the two sides, it is evident that one side is doped with N, while the other side is undoped. This uniquely verifies this heterojunction proof-of-concept based on an N-content of 0.002 at. % extracted from analysis discussed in a previous section. The use of Raman mapping, based on the

sensitivity of the G′ mode to the presence of N atoms in the lattice, is possibly the most sensitive probe for characterizing the formation of such heterostructures. Compared to heterojunction concepts that have been discussed on a single-molecule level, utilizing this self-assembled material enables the formation of heterojunctions that are self-assembled into highly aligned and densely packed architectures that are comprised of ultralong nanotubes. Therefore, the use of this process for self-assembled growth and dry transfer opens opportunities to fabricate complex material architectures that likely could not be assembled or organized utilizing other techniques (*i.e.*, such as growth and postgrowth solution-phase processing).

In the classical picture of n-doping of semiconducting SWNT with N atoms in the SWNNT arrays, one can envision this material to yield a structure whereby the Fermi level of the doped SWNT can be engineered such that the band bending at the interface between the SWNNT and the SWNT sides can be tuned (Supporting Information). The demonstration of the controlled doping levels ranging between 10^{-5} at. % and 1 at. % N emphasizes a wide range of tunability in the doping levels, and hence the built-in field at the interface of this junction. However, the presence of a minority of metallic SWNTs may act to complicate this simple picture, as it is unclear what effect N-doping can have on SWNTs with metallic character. Nonetheless, we expect that in combination with techniques such as hydrogenation (that acts to localize π electrons), or selective SWNT growth,[44,45] this material geometry could permit use in a variety of optical or photovoltaic devices that could be tuned for optimal device performance. Therefore, the ability to grow these self-assembled heterostructures and transfer them to large areas opens up new purely "bottom-up" opportunities for SWNT- or SWNNT-based applications. Such materials could provide tunable and efficient nanomaterial alternatives for conventional materials in a variety of important applications, in addition to creating materials on which new physics and chemistry can be explored and developed.

In conclusion, we demonstrate here a broad picture that encompasses the growth, characterization, and materials processing necessary for applications using N-doped SWNT arrays. We specifically determine that HCN plays a primary role as a precursor molecule in the growth of SWNNT arrays, analogous to the role of C_2H_2 in SWNT array growth. We then utilize optical characterization to (i) establish that the G′ mode is sensitive to N-atom concentrations down to 10^{-5} at. % N and (ii) establish a dependence of the E_{11}^{SC} mode in the optical absorption of the SWNNT arrays on N-content in the SWNNT. Finally, we demonstrate a framework for transfer printing of doped–undoped heterojunctions of SWNNT/SWNT self-assembled structures and verify this architecture using Raman mapping. This work opens up new concepts that are important for achieving controlled growth of self-assembled SWNNTs, characterizing the SWNNTs quantitatively using optical techniques, and fabricating complex material architectures that are of interest for advanced applications.

METHODS

C–N SWNT Growth. Nitrogen-doped SWNT arrays were grown using a modified supergrowth process described in previous works. This involved the use of 0.5% C_2H_2, 0.5% H_2O, and 99% H_2 gas mixture fixed at a pressure of ~1.4 Torr. As shown in Figure 1a, gas-phase N-containing precursors were introduced into the reaction chamber by loading liquid into a vacuum flask, three cycles of freeze–thawing using an acetone/dry ice bath under vacuum (to remove dissolved contaminants), and using the equilibrium vapor pressure of the precursor species when the vacuum flask is opened to the reaction gas flow. In our studies, we utilized C_5H_5N and CH_3CN (both purchased from Sigma-Aldrich, anhydrous 99.8%), which both have high vapor pressures at room temperature (~20 and ~80 mmHg), making this gas-phase route effective. The partial pressure of the N-containing precursor was measured assuming all gases behave as ideal gases and using a 100 Torr capacitance monometer to calibrate the number of turns on a low-flow Swagelock metering valve to the partial pressure. The relative amount of each N-containing precursor was also alternately confirmed using *in situ* mass spectrometry. In each case, the catalyst is reduced prior to growth using a hot tungsten filament, as described in detail elsewhere for processes designed for SWNT array growth. For the highest levels of N-doping, no C_2H_2 was utilized in the reaction flow, and only CH_3CN or C_5H_5N was utilized as the carbon and nitrogen source.

For most of our characterization, we utilized the conditions described here (total reaction pressure between 1.5 and 2 Torr). However, to achieve the ultralong SWNNT carpets that were found to grow up to 1.5 mm tall (Figure 1b), the pressure was elevated to ~25 Torr, which has been described in past work to yield the ultralong SWNT carpets more commonly associated with supergrowth (up to 3–4 mm for pristine SWNTs).

Instrumentation. SEM characterization of aligned SWNNTs was conducted using a FEI Quanta 400 environmental SEM. TEM characterization of the SWNNT material was performed utilizing a JEOL 2100 field emission gun TEM using 200 kV accelerating voltage. TEM samples were prepared by dry adhesion of SWNNTs to a TEM grid from a SWNNT array sample. *In situ* mass spectrometry studies were performed using a Dycor residual gas analyzer that was connected to the growth system through a bleed line and housed in an ultrahigh vacuum (~1×10^{-9} Torr) chamber. Raman spectroscopy studies were utilized using a Renishaw microRaman equipped with 514, 633, and 785 nm lasers. Infrared absorption measurements were carried out utilizing a Thermo Nicolet Nexus 870 FTIR system using an IR light source, DTGS detector, and KBr beamsplitter. Samples were prepared as discussed in detail previously,[27] and polarized absorption measurements were made utilizing a ZnSe polarizer placed in front of a cell where the sample (SWNNT arrays transferred to a KBr window) was placed between the polarizer and the detector.

For additional details about the experimental measurements regarding the growth and characterization of species

using mass spectrometry, the reader is referred to the Supporting Information.

Acknowledgment. The authors thank D. Natelson for use of equipment for catalyst evaporation, R. Bardhan for help with figures, A. Sristavia for illuminating discussions regarding doped CNTs, and S. Ripley for experimental assistance. This work was supported by the Lockheed Martin LANCER program and in part by AFOSR, the ONR MURI Program (00007666, N00014-09-1-1066), and the Department of Energy's Hydrogen Storage Program.

Supporting Information Available: Electron ionization mass spectrometry cracking patterns for N-containing precursors utilized and detailed experiments to establish role of HCN during growth, Raman D, G, and RBM mode characterization as a function of SWNT N-doping. This information is available free of charge *via* the Internet at http://pubs.acs.org.

REFERENCES AND NOTES

1. Elias, A. L.; Ayala, P.; Zamudio, A.; Grobosch, M.; Cruz-Silva, E.; Romo-Herrera, J. M.; Campos-Delgado, J.; Terrones, H.; Pichler, T.; Terrones, M. Spectroscopic Characterization of N-Doped Single-Walled Carbon Nanotube Strands: An X-Ray Photoelectron Spectroscopy and Raman Study. *J. Nanosci. Nanotechnol.* **2010**, *10*, 3959–3964.
2. Campos-Delgado, J.; Maciel, I. O.; Cullen, D. A.; Smith, D. J.; Jorio, A.; Pimenta, M. A.; Terrones, H.; Terrones, M. Chemical Vapor Deposition Synthesis of N-, P-, and Si-Doped Single-Walled Carbon Nanotubes. *ACS Nano* **2010**, *4*, 1696–1702.
3. Maciel, I. O.; Campos-Delgado, J.; Pimenta, M. A.; Terrones, M.; Terrones, H.; Rao, A. M.; Jorio, A. Boron, Nitrogen and Phosphorous Substitutionally Doped Single-Wall Carbon Nanotubes Studied by Resonance Raman Spectroscopy. *Phys. Status Solidi B* **2009**, *246*, 2432–2435.
4. Lin, H.; Arenal, R.; Enouz-Vedrenne, S.; Stephan, O.; Loiseau, A. Nitrogen Configuration in Individual Cnx-Swnts Synthesized by Laser Vaporization Technique. *J. Phys. Chem. C* **2009**, *113*, 9509–9511.
5. Lin, H.; Lagoute, J.; Chacon, C.; Arenal, R.; Stephan, O.; Repain, V.; Girard, Y.; Enouz, S.; Bresson, L.; Rousset, S.; *et al*. Combined Stm/Sts, Tem/Eels Investigation of Cnx-Swnts. *Phys. Status Solidi B* **2008**, *245*, 1986–1989.
6. Ayala, P.; Freire, F. L.; Rummeli, M. H.; Gruneis, A.; Pichler, T. Chemical Vapor Deposition of Functionalized Single-Walled Carbon Nanotubes with Defined Nitrogen Doping. *Phys. Status Solidi B* **2007**, *244*, 4051–4055.
7. Villalpando-Paez, F.; Zamudio, A.; Elias, A. L.; Son, H.; Barros, E. B.; Chou, S. G.; Kim, Y. A.; Muramatsu, H.; Hayashi, T.; Kong, J.; *et al*. Synthesis and Characterization of Long Strands of Nitrogen-Doped Single-Walled Carbon Nanotubes. *Chem. Phys. Lett.* **2006**, *424*, 345–352.
8. Glerup, M.; Steinmetz, J.; Samaille, D.; Stephan, O.; Enouz, S.; Loiseau, A.; Roth, S.; Bernier, P. Synthesis of N-Doped Swnt Using the Arc-Discharge Procedure. *Chem. Phys. Lett.* **2004**, *387*, 193–197.
9. Ayala, P.; Arenal, R.; Rummeli, M.; Rubio, A.; Pichler, T. The Doping of Carbon Nanotubes with Nitrogen and Their Potential Applications. *Carbon* **2010**, *48*, 575–586.
10. Gong, K. P.; Du, F.; Xia, Z. H.; Durstock, M.; Dai, L. M. Nitrogen-Doped Carbon Nanotube Arrays with High Electrocatalytic Activity for Oxygen Reduction. *Science* **2009**, *323*, 760–764.
11. Cruz-Silva, E.; Cullen, D. A.; Gu, L.; Romo-Herrera, J. M.; Munoz-Sandoval, E.; Lopez-Urias, F.; Sumpter, B. G.; Meunier, V.; Charlier, J. C.; Smith, D. J.; *et al*. Heterodoped Nanotubes: Theory, Synthesis, and Characterization of Phosphorus-Nitrogen Doped Multiwalled Carbon Nanotubes. *ACS Nano* **2008**, *2*, 441–448.
12. Sumpter, B. G.; Meunier, V.; Romo-Herrera, J. M.; Cruz-Silva, E.; Cullen, D. A.; Terrones, H.; Smith, D. J.; Terrones, M. Nitrogen-Mediated Carbon Nanotube Growth: Diameter Reduction, Metallicity, Bundle Dispersability, and Bamboo-Like Structure Formation. *ACS Nano* **2007**, *1*, 369–375.
13. Enouz, S.; Bantignies, J. L.; Babaa, M. R.; Alvarez, L.; Parent, P.; Le Normand, F.; Stephan, O.; Poncharal, P.; Loiseau, A.; Doyle, B. P. Spectroscopic Study of Nitrogen Doping of Multi-Walled Carbon Nanotubes. *J. Nanosci. Nanotechnol.* **2007**, *7*, 3524–3527.
14. Ayala, P.; Gruneis, A.; Kramberger, C.; Rummeli, M. H.; Solorzano, I. G.; Freire, F. L.; Pichler, T. Effects of the Reaction Atmosphere Composition on the Synthesis of Single and Multiwalled Nitrogen-Doped Nanotubes. *J. Chem. Phys.* **2007**, *127*, 6.
15. Ayala, P.; Grueneis, A.; Gemming, T.; Grimm, D.; Kramberger, C.; Ruemmeli, M. H.; Freire, F. L.; Kuzmany, H.; Pfeiffer, R.; Barreiro, A.; *et al*. Tailoring N-Doped Single and Double Wall Carbon Nanotubes from a Nondiluted Carbon/Nitrogen Feedstock. *J. Phys. Chem. C* **2007**, *111*, 2879–2884.
16. Ayala, P.; Grueneis, A.; Gemming, T.; Buchner, B.; Rummeli, M. H.; Grimm, D.; Schumann, J.; Kaltofen, R.; Freire, F. L.; Fonseca, H. D.; *et al*. Influence of the Catalyst Hydrogen Pretreatment on the Growth of Vertically Aligned Nitrogen-Doped Carbon Nanotubes. *Chem. Mater.* **2007**, *19*, 6131–6137.
17. Ewels, C. P.; Glerup, M. Nitrogen Doping in Carbon Nanotubes. *J. Nanosci. Nanotechnol.* **2005**, *5*, 1345–1363.
18. Jang, J. W.; Lee, C. E.; Lyu, S. C.; Lee, T. J.; Lee, C. J. Structural Study of Nitrogen-Doping Effects in Bamboo-Shaped Multiwalled Carbon Nanotubes. *Appl. Phys. Lett.* **2004**, *84*, 2877–2879.
19. Terrones, M.; Ajayan, P. M.; Banhart, F.; Blase, X.; Carroll, D. L.; Charlier, J. C.; Czerw, R.; Foley, B.; Grobert, N.; Kamalakaran, R.; *et al*. N-Doping and Coalescence of Carbon Nanotubes: Synthesis and Electronic Properties. *Appl. Phys. A-Mater. Sci. Process.* **2002**, *74*, 355–361.
20. Ibrahim, E. M. M.; Khavrus, V. O.; Leonhardt, A.; Hampel, S.; Oswald, S.; Rummeli, M. H.; Buchner, B. Synthesis, Characterization, and Electrical Properties of Nitrogen-Doped Single-Walled Carbon Nanotubes with Different Nitrogen Content. *Diam. Relat. Mater.* **2010**, *19*, 1199–1206.
21. Liu, J.; Zhang, Y.; Ionescu, M. I.; Li, R. Y.; Sun, X. L. Nitrogen-Doped Carbon Nanotubes with Tunable Structure and High Yield Produced by Ultrasonic Spray Pyrolysis. *Appl. Surf. Sci.* **2011**, *257*, 7837–7844.
22. Nxumalo, E. N.; Letsoalo, P. J.; Cele, L. M.; Coville, N. J. The Influence of Nitrogen Sources on Nitrogen Doped Multi-Walled Carbon Nanotubes. *J. Organomet. Chem.* **2010**, *695*, 2596–2602.
23. Yasuda, S.; Futaba, D. N.; Yamada, T.; Satou, J.; Shibuya, A.; Takai, H.; Arakawa, K.; Yumura, M.; Hata, K. Improved and Large Area Single-Walled Carbon Nanotube Forest Growth by Controlling the Gas Flow Direction. *ACS Nano* **2009**, *3*, 4164–4170.
24. Hata, K.; Futaba, D. N.; Mizuno, K.; Namai, T.; Yumura, M.; Iijima, S. Water-Assisted Highly Efficient Synthesis of Impurity-Free Single-Waited Carbon Nanotubes. *Science* **2004**, *306*, 1362–1364.
25. Kim, S. M.; Pint, C. L.; Amama, P. B.; Zakharov, D. N.; Hauge, R. H.; Maruyama, B.; Stach, E. A. Evolution in Catalyst Morphology Leads to Carbon Nanotube Growth Termination. *J. Phys. Chem. Lett.* **2010**, *1*, 918–922.
26. Amama, P. B.; Pint, C. L.; McJilton, L.; Kim, S. M.; Stach, E. A.; Murray, P. T.; Hauge, R. H.; Maruyama, B. Role of Water in Super Growth of Single-Walled Carbon Nanotube Carpets. *Nano Lett.* **2009**, *9*, 44–49.
27. Pint, C. L.; Xu, Y. Q.; Moghazy, S.; Cherukuri, T.; Alvarez, N. T.; Haroz, E. H.; Mahzooni, S.; Doorn, S. K.; Kono, J.; Pasquali, M.; *et al*. Dry Contact Transfer Printing of Aligned Carbon Nanotube Patterns and Characterization of Their Optical Properties for Diameter Distribution and Alignment. *ACS Nano* **2010**, *4*, 1131–1145.
28. Nessim, G. D.; Seita, M.; Plata, D. L.; O'Brien, K. P.; Hart, A. J.; Meshot, E. R.; Reddy, C. M.; Gschwend, P. M.; Thompson, C. V. Precursor Gas Chemistry Determines the Crystallinity of Carbon Nanotubes Synthesized at Low Temperature. *Carbon* **2011**, *49*, 804–810.
29. Plata, D. L.; Hart, A. J.; Reddy, C. M.; Gschwend, P. M. Early Evaluation of Potential Environmental Impacts of Carbon

Nanotube Synthesis by Chemical Vapor Deposition. *Environ. Sci. Technol.* **2009**, *43*, 8367–8373.
30. Meshot, E. R.; Plata, D. L.; Tawfick, S.; Zhang, Y. Y.; Verploegen, E. A.; Hart, A. J. Engineering Vertically Aligned Carbon Nanotube Growth by Decoupled Thermal Treatment of Precursor and Catalyst. *ACS Nano* **2009**, *3*, 2477–2486.
31. Plata, D. L.; Meshot, E. R.; Reddy, C. M.; Hart, A. J.; Gschwend, P. M. Multiple Alkynes React with Ethylene to Enhance Carbon Nanotube Synthesis, Suggesting a Polymerization-Like Formation Mechanism. *ACS Nano* **2010**, *4*, 7185–7192.
32. Zhou, J.; Wang, J.; Liu, H.; Banis, M. H.; Sun, X.; Sham, T.-K. Imaging Nitrogen in Individual Carbon Nanotubes. *J. Phys. Chem. Lett.* **2010**, *1*, 1709–1713.
33. Maciel, I. O.; Anderson, N.; Pimenta, M. A.; Hartschuh, A.; Qian, H. H.; Terrones, M.; Terrones, H.; Campos-Delgado, J.; Rao, A. M.; Novotny, L.; *et al*. Electron and Phonon Renormalization near Charged Defects in Carbon Nanotubes. *Nat. Mater.* **2008**, *7*, 878–883.
34. Pint, C. L.; Kim, S. M.; Stach, E. A.; Hauge, R. H. Rapid and Scalable Reduction of Dense Surface-Supported Metal-Oxide Catalyst with Hydrazine Vapor. *ACS Nano* **2009**, *3*, 1897–1905.
35. Zhong, G.; Hofmann, S.; Yan, F.; Telg, H.; Warner, J. H.; Eder, D.; Thomsen, C.; Milne, W. I.; Robertson, J. Acetylene: A Key Growth Precursor for Single-Walled Carbon Nanotube Forests. *J. Phys. Chem. C* **2009**, *113*, 17321–17325.
36. Pint, C. L.; Pheasant, S. T.; Parra-Vasquez, A. N. G.; Horton, C.; Xu, Y. Q.; Hauge, R. H. Investigation of Optimal Parameters for Oxide-Assisted Growth of Vertically Aligned Single-Walled Carbon Nanotubes. *J. Phys. Chem. C* **2009**, *113*, 4125–4133.
37. Eres, G.; Kinkhabwala, A. A.; Cui, H. T.; Geohegan, D. B.; Puretzky, A. A.; Lowndes, D. H. Molecular Beam-Controlled Nucleation and Growth of Vertically Aligned Single-Wall Carbon Nanotube Arrays. *J. Phys. Chem. B* **2005**, *109*, 16684–16694.
38. Xu, Y. Q.; Flor, E.; Schmidt, H.; Smalley, R. E.; Hauge, R. H. Effects of Atomic Hydrogen and Active Carbon Species in 1 Mm Vertically Aligned Single-Walled Carbon Nanotube Growth. *Appl. Phys. Lett.* **2006**, *89*, 3.
39. Eres, G.; Rouleau, C. M.; Yoon, M.; Puretzky, A. A.; Jackson, J. J.; Geohegan, D. B. Model for Self-Assembly of Carbon Nanotubes from Acetylene Based on Real-Time Studies of Vertically Aligned Growth Kinetics. *J. Phys. Chem. C* **2009**, *113*, 15484–15491.
40. Houser, T. J.; McCarville, M. E.; Biftu, T. Kinetics of the Thermal-Decomposition of Pyridine in a Flow System. *Int. J. Chem. Kinet.* **1980**, *12*, 555–568.
41. Houser, T. J.; Hull, M.; Alway, R. M.; Biftu, T. Kinetics of the Formation of HCN during Pyridine Pyrolysis. *Int. J. Chem. Kinet.* **1980**, *12*, 569–574.
42. Spataru, C. D. Leonard, F., Tunable Bandgaps and Excitons in Doped Semiconducting Carbon Nanotubes Made Possible by Acoustic Plasmons. *Phys. Rev. Lett.* **2010**, *104*, 177402.
43. Pint, C. L.; Xu, Y. Q.; Pasquali, M.; Hauge, R. H. Formation of Highly Dense Aligned Ribbons and Transparent Films of Single-Walled Carbon Nanotubes Directly from Carpets. *ACS Nano* **2008**, *2*, 1871–1878.
44. Hong, G.; Zhang, B.; Peng, B. H.; Zhang, J.; Choi, W. M.; Choi, J. Y.; Kim, J. M.; Liu, Z. F. Direct Growth of Semiconducting Single-Walled Carbon Nanotube Array. *J. Am. Chem. Soc.* **2009**, *131*, 14642–14643.
45. Ding, L.; Tselev, A.; Wang, J. Y.; Yuan, D. N.; Chu, H. B.; McNicholas, T. P.; Li, Y.; Liu, J. Selective Growth of Well-Aligned Semiconducting Single-Walled Carbon Nanotubes. *Nano Lett.* **2009**, *9*, 800–805.